Journal of Solid State Electrochemistry (2019) 23:1109–1119
https://doi.org/10.1007/s10008-018-04183-4

ORIGINAL PAPER

The effect of alkyl chain of the imidazolium ring on the poly(o-methoxyaniline)/ionic liquid supercapacitor performance

L. G. da Trindade[1,2] · W. A. Christinelli[3] · L. Zanchet[2] · D. Coelho[1] · A. B. Trench[1] · Emilse M. A. Martini[2] · Daniel S. Correa[3] · Luiz H. C. Mattoso[3] · E. C. Pereira[1]

Received: 1 November 2018 / Revised: 14 December 2018 / Accepted: 19 December 2018 / Published online: 2 February 2019
© Springer-Verlag GmbH Germany, part of Springer Nature 2018

Abstract

New materials can be developed using a known compound with enhanced properties modifying and controlling its microstructure, morphology, and density of defects. In this work, a new material was produced by the addition of ionic liquid (IL) to the poly(o-methoxyaniline) (POMA) conductive polymer, in the form of esmeraldine salt. The polymer impregnated with IL was tested as an electrode for use in supercapacitors. The results show that the charge storage properties of the materials are dependent on the length of the alquil substituent of imidazolium ring of ionic liquid cation. The best results, obtained by the addition of 1-butyl-3-methylimidazolium triflate IL to the polymer, improved electrical charge storage and electrochemical stability, making the material a promising electrode for supercapacitor devices. This compound has specific capacitance of 205 F/g, five times larger than pure POMA and was stable for 3000 cycles of charge/discharge experiments carried out at 1.0 A/g.

Keywords Conducting polymers · Poly(o-methoxyaniline) · Supercapacitors · Ionic liquids

Introduction

Conducting polymers, CPs, are an important class of functional organic materials that can be used in electronic, optical, and electrochemical devices. Among the different fields of applications, new materials for energy conversion and storage are an important one aiming to decrease the environmental impact of the nowadays most used energy sources [1–3]. In this sense, supercapacitors have been proposed as significant alternative devices for energy storage. Supercapacitors that store energy from redox processes are called pseudocapacitors and can be produced from conductive polymers. When used as a positive electrode, the polymer oxidizes, and the holes generated along the chain are balanced by the input of anions (p doping) and this is a reversible reaction [4]. Polyaniline (PANI) is one of the conducting polymers that have been widely studied to be used in supercapacitors due to its good chemical stability and low cost [5]. Conduction in PANI occurs through the acid/base doping mechanism, i.e., through protonation and internal redox process. Despite the numerous advantages of PANI, its use is limited due to its low processability [6]. The substitution, in the aromatic ring of aniline, with electron donating groups improves its solubility and processability. Previous studies suggest that higher levels of conductivity can be obtained when the aniline is replaced with alkoxy groups that are electron donors. Thus, the coulomb interactions between the positive charges of the polymer chain are reduced, increasing the electronic delocalization and, consequently, the electrical conductivity. These materials can be positively charged (p-doped polymer) and, considering their porosity and soft material characteristics, the double-layer capacitance also contributes to the high values of the total capacitance obtained using this polymer [7]. In recent years, different chemical modifications have been reported to improve the properties of

Electronic supplementary material The online version of this article (https://doi.org/10.1007/s10008-018-04183-4) contains supplementary material, which is available to authorized users.

✉ E. C. Pereira
ernesto@ufscar.br

[1] Chemistry Department, Federal University of São Carlos, C.P. 676, São Carlos, SP 13560-970, Brazil

[2] Institute of Chemistry, UFRGS, Av. Bento Gonçalves 9500, 91501-970, P.O. Box 15003, Porto Alegre, RS, Brazil

[3] Nanotechnology National Laboratory for Agriculture (LNNA), Embrapa Instrumentation, São Carlos, SP 13560-970, Brazil

conjugated polymers aiming to attend those characteristics required for technological applications. The enhancement of the efficiency and durability of devices based on CPs can be achieved by the modification of the device design or by optimizing the material synthesis, which leads to improved properties [8–13]. The modification of the synthesis of CPs can provide high efficiency and stability, increasing the possibilities of technological applications. Furthermore, the addition of ILs to the polymeric samples is an alternative to optimize their properties [14]. ILs are organic salts with large cations and anions with melting point less than 100 °C [15]. Due to their favorable properties such as negligible vapor pressure, low flammability, high ionic conductivity, wide electrochemical window, and excellent thermal and chemical stability [16], ILs are used in different applications, such as organic electrolytes for electrochemical devices [17], liquid-liquid extraction [18], batteries [19], fuel cells [20], and supercapacitors [21, 22]. However, many ionic liquids have low ionic conductivity due to the relative size of their ions and the high viscosity. As ionic conductivity is a fundamental parameter to design electrochemical devices, several researches have been done to develop new ionic liquids with a wider electrochemical window and better ionic conductivity [23, 24]. However, the great majority of electric double-layer capacitors (EDLCs) designed with ionic liquids have relatively low capacity and power, leaving room for the development of new capacitors with ionic liquid with better performance. Ketabi et al. [25] developed non-aqueous polymer electrolytes based on the protic ionic liquids (PIL). The polymeric matrix was poly (ethylene oxide) (PEO) and the PIL were 1-ethyl-3-methylimidazolium hydrogensulfate ($EMIHSO_4$), 1-methylimidazolium hydrogensulfate ($MIHSO_4$), and imidazolium hydrogensulfate ($ImHSO_4$). They observed that the pseudocapacitance was higher for the cell with PEO-$MIHSO_4$-$ImHSO_4$ (59 mF/cm^2) over that of PEO-$EMIHSO_4$-$ImHSO_4$ (43 mF/cm^2), which suggests that $MIHSO_4$-$ImHSO_4$ has a higher proton contribution to the polymer system than $EMIHSO_4$-$ImHSO_4$. Kim et al. [26] synthesized reduced graphene oxide with different weight ratios of 1-butyl-3-methylimidazolium hexafluorophosphate IL (rGO/IL) and then tested in 6-M aqueous KOH electrolyte. Among the samples, the rGO/IL (1:7) showed the highest specific capacitance of 148 F/g while the sample rGO exhibits specific capacitance equal to 82 F/g under the same conditions. The authors concluded that the combination of IL with rGO enhanced the electrochemical performance of pure rGO presumably because the IL enhanced the charge transport by facilitating ion diffusion. The present work reports the preparation, characterization, and comparative application of three ILs, namely, 1-butyl-3-methylimidazolium triflate ($C_4MI.CF_3SO_3$), 1-decyl-3-methylimidazolium triflate ($C_{10}MI.CF_3SO_3$), and 1-hexadecyl-3-methylimidazolium triflate ($C_{16}MI.CF_3SO_3$), in the POMA structure for supercapacitor applications. The imidazolium ring of the IL cation has delocalized electrons that can increase the electronic conductivity of the polymer. Likewise, the $CF_3SO_3^-$ anion, similar to the polar termination of the Nafion®, can also aid in increasing the ionic conductivity, improving POMA charge/discharge processes. The different cations were tested because the increase of the alkyl chain can bind to the POMA chain by Van der Waals forces and make it difficult to leach the ionic liquid. The electrochemical performances of POMA/IL supercapacitors have been evaluated and compared with pristine POMA supercapacitor.

Experiment

Materials and methods

The poly(o-methoxy aniline) in the form of esmeraldine salt, also known as anisidine, has been synthesized by direct chemical oxidation of the monomer as described by Mattoso [27]. POMA (Fig. 1) solution was prepared by dissolving 20 mg of POMA in a mixture of H_2O and acetonitrile (ACN) in a proportion of 59:1 (*v*/*v*). ACN was used to enhance the solubility of the polymer in water. All the reactants were supplied by Sigma-Aldrich, and anisidine monomer was used after distillation. Analytical-grade lithium perchlorate (Sigma-Aldrich) and polyethylene glycol (PEG) (Synth) were used for the electrochemical characterizations. The ILs 1-butyl-3-methylimidazolium triflate, 1-decyl-3-methylimidazolium triflate, and 1-hexadecyl-3-methylimidazolium triflate, which chemical structures are shown in Fig. 1, were synthesized as previously described [28, 29]. POMA/IL electrodes were prepared using *casting* method by mixing the corresponding IL in the ratio 4:1 POMA:IL. Then, 250 μL of the solution was deposited onto glass substrates coated with indium tin oxide (ITO) electrode, leading to a polymeric film with 38 ± 2 μg (area = 1 cm^2). These substrates were previously etched with a $H_2O_2/NH_4OH/H_2O$ [1:1:5 (*v*/*v*)] solution and ultrapure water (Milli-Q system) to prepare a hydrophilic surface. For the electrochemical experiments, an Ag pseudo-reference and Pt sheet (area 1 cm^2) were used as reference and counterelectrodes, respectively. In Table 1, the details of the sample compositions and sample designations are presented.

Characterization

The structures of PEG, POMA, C4-POMA, C10-POMA, and C16-POMA films were analyzed by attenuated total reflectance Fourier transform infrared (ATR-FTIR) spectroscopy (Bruker Alpha-P) between 4000 and 500 cm. Contact angle data were collected using a Kruss DSA 30 and the Drop Shape Analysis System software and analyzed by the Surftens 4.5 software. All measurements were carried out at room temperature with deionized water. The film morphologies were investigated by profilometer measurements, using a Bruker-

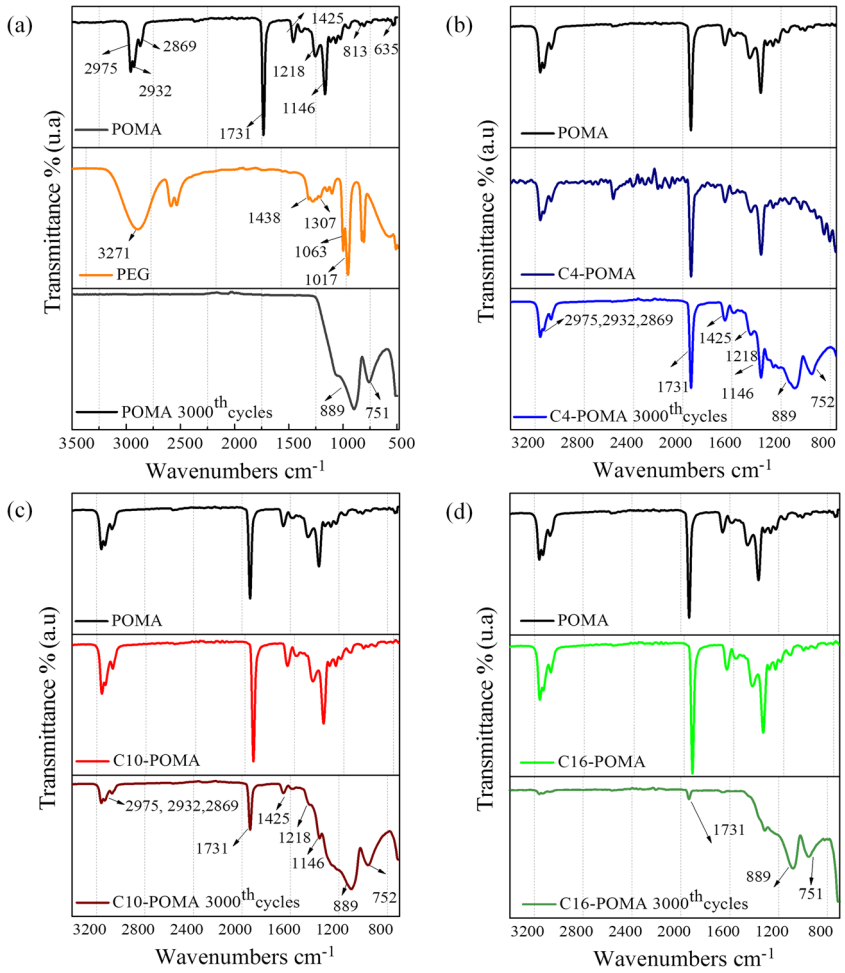

Fig. 1 ATR-FTIR spectra of POMA (**a**), C4-POMA (**b**), C10-POMA (**c**), and C16-POMA (**d**) pristine and after 3000th CV cycles

ContourGT-3D Optical Profiler. Electrochemical experiments were carried out in a three-electrode glass cell using an Autolab PGSTAT 302N. The measurements were carried out in PEG with 0.1 M $LiClO_4$. The electrochemical stability of the electrode with polymeric film has been studied using both galvanostatic and cyclic voltammetry experiments. All measurements were carried out at room temperature. For galvanostatic charge/discharge cycling, the load current was 1.0 A/g. Cyclic voltammetry characteristics of films were recorded after 100 charge/discharge cycles at 20 mV/s from − 0.2 to 0.3 V vs. Ag. The specific discharge capacitance of the active materials (C_{sp}) was obtained from galvanostatic charge-discharge curves, according to the relation [5]: $C_{sp} = \frac{I}{m\left(\frac{dV}{dt}\right)}$, where I is the applied current (A), m is the average mass of electrode materials, dV represents the potential change of a discharging process excluding the internal resistance drop (IR drop) occurring at the beginning of the cell discharge, and dt is the time interval of discharging process. The dV/dt is determined from the slope of the discharge curve. Specific power, P (W/kg), and specific energy, E (W h kg^{-1}), were obtained using the following equations [5, 30]: $P = \frac{I}{2}\frac{dV}{m}1000$ $E = \frac{C_{sp}\ (dV)^2}{2}\ \frac{1000}{3600}$. The electrochemical impedance spectroscopy (EIS) was performed in a conventional three-electrode cell at 25 °C in PEG with 0.1 M $LiClO_4$. The EIS was performed in the open-circuit potential (OCP), between frequencies of 100 mHz and 100 kHz, with amplitude of 10 mV. The equivalent electronic circuit was simulated using NOVA software (Metrohm-Autolab).

Table 1 Composition and sample designation of the POMA/IL electrodes

Sample designation	POMA (mg)	Ionic liquid	Ionic liquid (wt.%)
C4-POMA	20	$C_4MI.CF_3SO_3$	20
C10-POMA	20	$C_{10}MI.CF_3SO_3$	20
C16-POMA	20	$C_{16}MI.CF_3SO_3$	20

Results and discussions

Figure 1 shows the ATR-FTIR (before the 1st and after the 3000th cycles in PEG as solvent at 20 mV/s) for POMA, C4-POMA, C10-POMA, and C16-POMA. The spectrum of

POMA (Fig. 1a) presents characteristic peaks at 2975, 2932, and 2869 cm that can be attributed to the C–H stretching vibration in the methoxy group (–OCH_3) at the orthoposition of the phenylene ring [31]. The peaks that appeared at 1146, 1218, and 1425 cm and 1731 cm can be attributed to out-of-plane bending vibration, (CN) stretch vibration for benzenoid and quinoid rings of primary aromatic amines, and (C=N) or (C=C) linkage elongation of the aromatic compounds, respectively [32]. The vibration band of 813 and 625 cm could be attributed to substitution of the benzene ring [33]. For PEG, the bands observed could be assigned as follows: broadband near 3271 cm related to O–H groups, the deformation vibration of the C–H bonds at 1438 and 1380 cm, and the C–O bonding of the elongation vibration between 1063 and 1017 cm [34]. After 3000th cycles, the POMA only those bands at 889 and 751 cm are observed. According to Mamma et al. [35], in this range, the widening of the bands due to the insertion of dopants occurs; then, one possibility to explain this change is the entrance of the PEG in the film. The ATR-FTIR spectra for C4-POMA, C10-POMA, and C16-POMA are shown in Fig. 1b–d, respectively, before and after cycling. Sample C4-POMA (Fig. 1b) shows that after the cycling those bands characteristic of pure POMA remain, and in the region of 1146–752 cm, an enlargement is observed, indicating that the electrolyte could be entered in the film. For C10-POMA (Fig. 1c), after the cycling, the characteristic bands of C10-POMA are also observed with low intensity. In the same region observed in sample C4-POMA, it is observed an enlargement which could also be an indication of the electrolyte insertion in the film. However, a different behavior occurs for C16-POMA, where after the cycling the characteristic peaks of C16-POMA disappear, remaining only the band at 1731 cm (with low intensity) and the bands 889 and 751 cm, equal to pure POMA after cycling. This behavior could support the proposition that C16-POMA loses its properties as well as pure POMA after cycling.

Figure 2 shows the 1st and the 3000th voltametric cycle in PEG as solvent at 20 mV/s for POMA, C4-POMA, C10-POMA, and C16-POMA. The electrochemical performance of POMA and POMA/IL capacitors is also studied by varying the scan rate (Fig. S1). Figure S1 shows that the CV is dependent on the scan rate, which is characteristic of a capacitor [36]. The voltammogram exhibits an almost rectangular shape at low scanning speed. However, when the scan rate is high, the CV curve is deviated slightly due to the finite value of the equivalent series resistance in the EDLC [37]. In Fig. 2, the first CV curves of all samples show that the output current of C4-POMA is approximately 2.2 times greater than the pure POMA and the other samples. This result indicates that the modification of the polymer with $C_4MI.CF_3SO_3$ IL improves the POMA performance. It can also be observed that there is a decrease in the mass-normalized current as the imidazolium ring alkyl chain is larger, which could be attributed to the formation of small number of solvation cells around electrolyte ions [38]. However, after 3000 cycles, a decrease in the current was observed for all samples, which could be explained by the fact that during the cycling the electrolyte may be entertaining in the film, as indicated by the ATR-FTIR analyses.

Figure 3 shows the contact angle of all pristine samples and after 3000th cycles in PEG. The contact angle of the pure POMA in the pristine sample was not significantly different (74.5°) than that of the value measured after the 3000 cycles (72.8°), indicating that wettability does not change [39]. This behavior indicates that no important change in the wettability occurs, and, then, there is not any important charge accumulation or material degradation occurs. The voltammetric curves also support this proposition. However, for those the samples modified with the IL, it is possible to observe a significant change in the contact angle as the aging process occurs. C4-POMA contact angle changes from 84.3° to 52.6°, indicating that the surface of the sample has become more hydrophilic. Then, it is possible to propose that this change helps the film to maintain its properties during the aging process. However, for those films modified with $C_{10}MI.CF_3SO_3$ or $C_{16}MI.CF_3SO_3$, a reverse result was observed. The pristine films have more hydrophilic surfaces, 45.8° and 18.7°, respectively, for C10-POMA and C16-POMA, but after cycling, the contact angles changes to 61.6° and 78.2°, indicating that the films have become less hydrophilic.

Figure S3 shows the topographic analysis of the surfaces of POMA, C4-POMA, C10-POMA, and C16-POMA films obtained from profilometer measurements. The surface profile of the pure POMA film is rather flat, with the average surface roughness of 34.5 ± 0.03 nm. However, when the film is cycled 3000 times in PEG, the aging of the film causes a surface rearrangement with increasing of average surface roughness to 319.0 ± 0.09 nm. When the polymer was modified with the IL, the roughness has an increase of about 1.55 (50.3 ± 0.09 nm), 2.15 (70.0 ± 0.04 nm), and 2.57 (83.4 ± 0.07 nm) times, for the samples C4-POMA, C10-POMA, and C16-POMA, respectively, compared to unmodified film. However, after the aging of modified films (3000 cycles), a reduction in surface roughness for the C4-POMA (36.1 ± 0.10 nm) and C10-POMA (28.0 ± 0.06 nm) films is observed. Already the film C16-POMA (91.1 ± 0.03 nm) presents an increase of the roughness of the surface after the aging. All of these profile surface changes before aging may be associated with phase rearrangement of hydrophilic and hydrophobic regions in the POMA film microstructure during the formation of homogeneous POMA-IL films. However, the surface modifications presented after aging, besides being associated with the phase rearrangement of hydrophilic and hydrophobic regions, may have been caused by charge accumulation or material degradation. The electrochemical behavior of the films has been investigated using cyclic voltammetry and

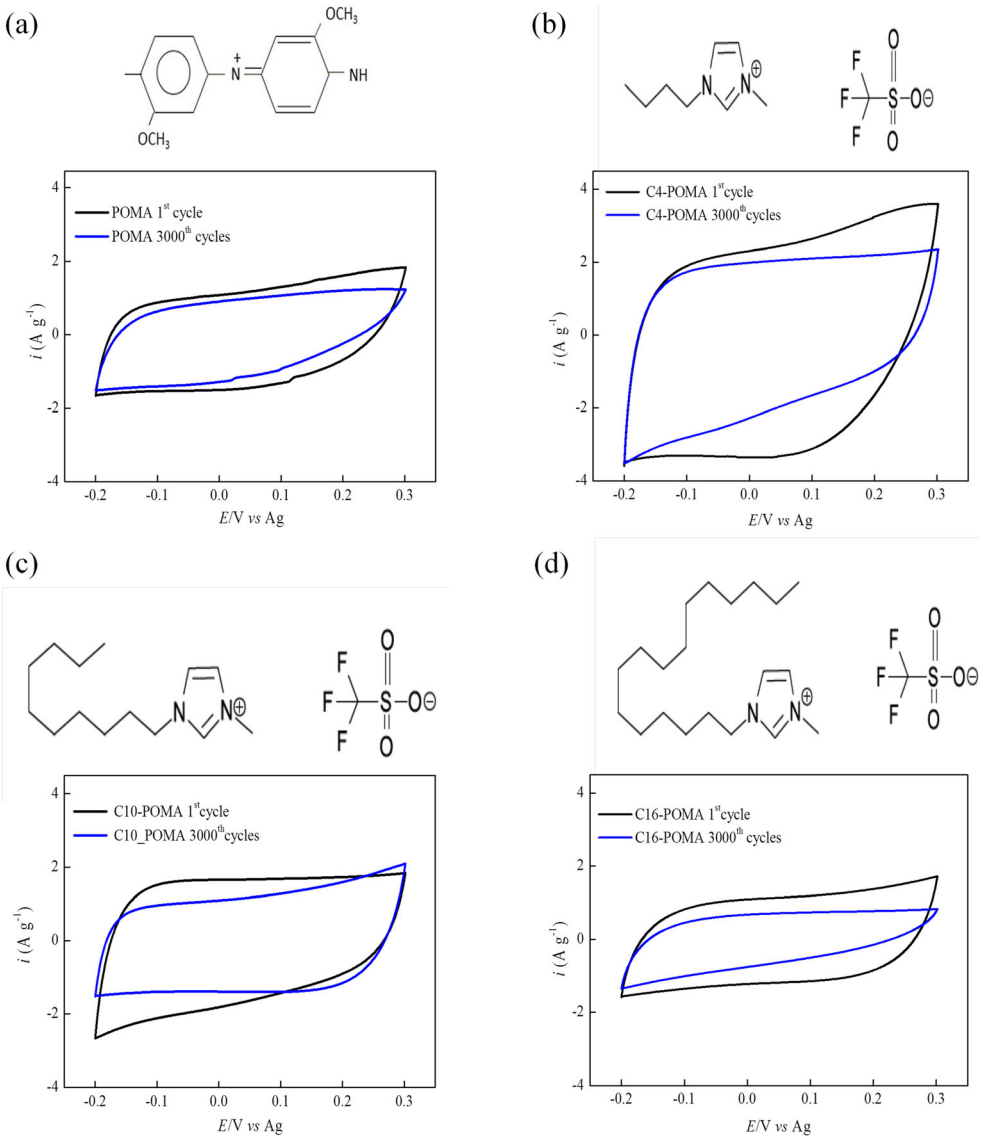

Fig. 2 Chemical structure and CV curves of POMA (**a**), chemical structure of $C_4MI.CF_3SO_3$ IL and CV curves of C4-POMA (**b**), chemical structure of $C_{10}MI.CF_3SO_3$ IL and CV curves of C10-POMA (**c**), and chemical structure of $C_{16}MI.CF_3SO_3$ IL and CV curves of C16-POMA (**d**)

charge/discharge experiments. To select the suitable density current, studies of charge/discharge profiles under different current densities were performed (Fig. S2). Figure 4a presents the CV of the samples in 0.1 M $LiClO_4$ + PEG solution. The potential was swept from − 0.2 to 0.3 V, where it is described in the literature that the POMA first redox pair appears, corresponding to the oxidation of leucoesmeraldine base to esmeraldine salt polaron form, as shown in Scheme 1 [40]. No remarkable differences among the voltamograms profiles can be observed, except for the values of specific current densities, i.e., the current density normalized by the material mass. Using CV data, the highest calculated specific capacitance value is 164 F/g for sample C4-POMA sample.

The increase of the specific current for sample modified by $C4MI.CF_3SO_3$ IL can be explained by an increase in hydrophilicity (Fig. 3). Considering that polymers are soft materials with large amount of solvent and IL among the chains, possibly C4 molecules, due to their size, the interface between the solution and the polymer chains could be increased. Certainly, at this point it is important to question why the specific currents decrease when $C10MI.CF_3SO_3$ or $C16MI.CF_3SO_3$ ILs are used. One hypothesis to explain this fact is that the increase in the alkyl chain of the ILs leads to a decrease in the hydrophilicity, which causes an increase in the resistance to the entrance of the counterion, leading to a decrease of the specific current of the samples. Figure 4b represents C/D profile at a current density of 2.0 A/g and a potential range between − 0.2 and 0.3 V (vs. Ag) for all samples. All samples exhibit a triangular linear profile, typical of electric-double layer capacitors, and the slopes of the discharge curves, which are inversely proportional to the capacitances, are similar in all cases. Figure 4c presents the calculated values for the specific capacitances under different experimental conditions using C/D curves. As expected, there is a smooth

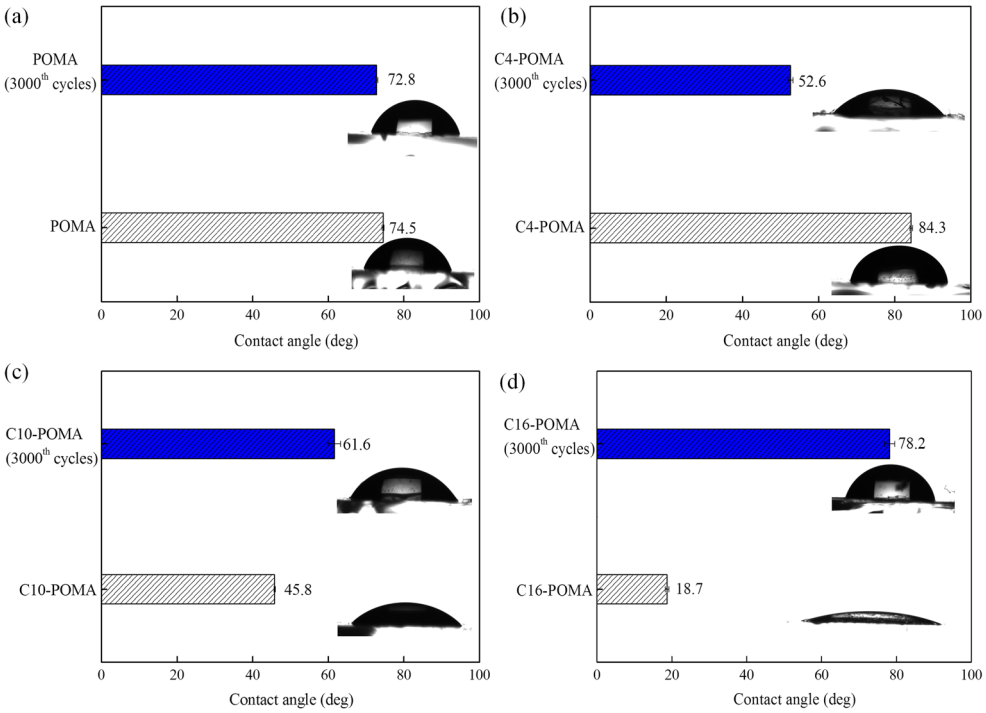

Fig. 3 Contact angle of **a** POMA, **b** C4-POMA, **c** C10-POMA, and **d** C16-POMA of pristine samples and after 3000th cycles in PEG at ambient temperature

decrease in the specific capacitance when the sweep rate or the applied current increases. C4-POMA samples present values that are three to five times higher than the other samples. These results are summarized in the Ragone plot (Fig. 4d). As can be observed, in agreement to those data in Fig. 4, C4-POMA sample presents the best results. The obtained value for specific energy is 2.5 W h kg^{-1}, whereas the values for specific power are constant for all the experimental conditions measured. By analyzing the data described previously, was investigated the electrochemical aging of C4-POMA film using charge/discharge measurements. The galvanostatic charge/discharge experiments were carried out at a current

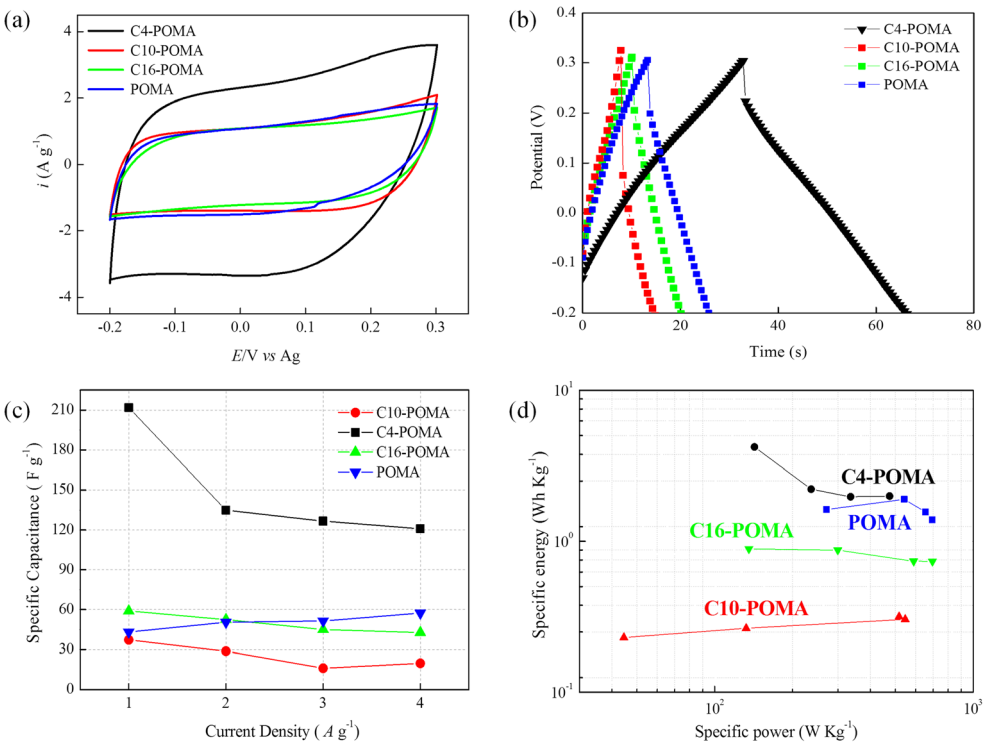

Fig. 4 **a** Cyclic voltammetry. **b** Charge/discharge measurements at 2 A/g. **c** Specific capacitance in function as current density. **d** Ragone plot of POMA, C4-POMA, C10-POMA, and C16-POMA films. Measurements were made at room temperature

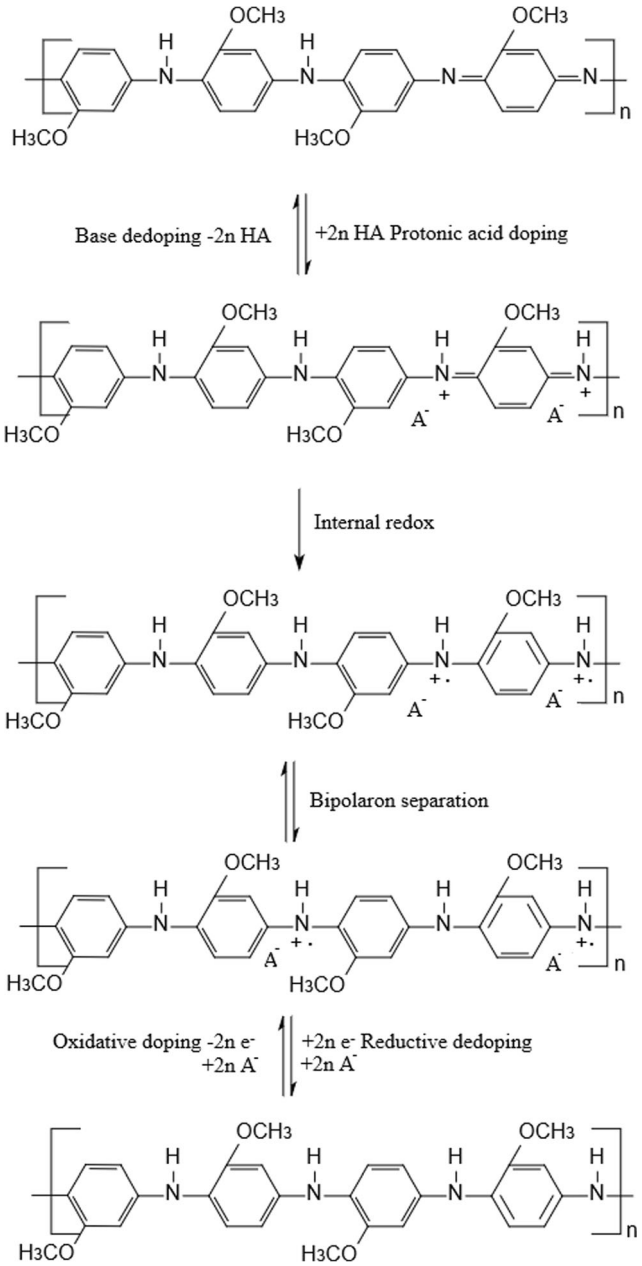

Scheme 1 Oxidative doping of leucoemeraldine base and protonic acid doping of emeraldine base, where A^- is an anion

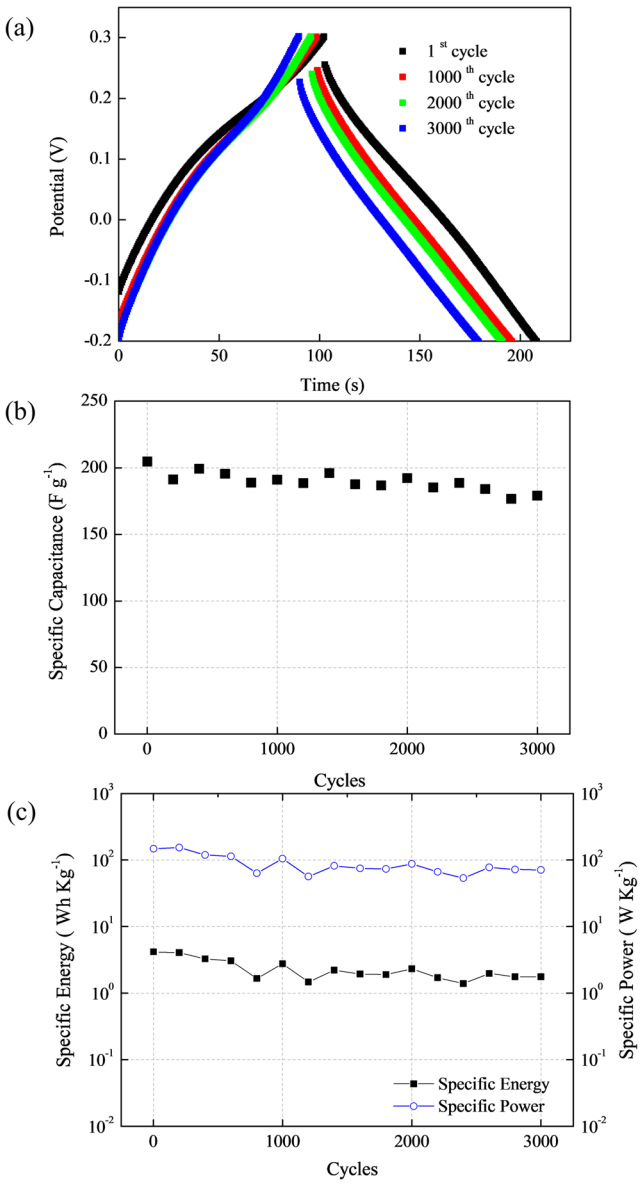

Fig. 5 Charge/discharge characterization of C4-POMA. **a** Charge-discharge profiles from −0.2 to 0.3 V. **b** Specific capacitance during 3000 cycles. **c** Specific energy and power during 3000 cycles of C4-POMA

density of 1.0 A/g and a potential range between −0.2 and 0.3 V (vs. Ag) during 3000 cycles. As can be observed in Fig. 5a, there is a small change in the slope of the discharge part of the curve after 3000 cycles suggesting a good stability of the material. C4-POMA film is stable for 3000 cycles, which is considerably higher than pure POMA using common counter ions. In Fig. 5b, C4-POMA has a specific capacitance of 205 F/g at the beginning of charge/discharge measurement, and, after 3000 cycles, this value falls to 180 F/g. These results show that C4-POMA presents retention of 87% of specific capacitance value during aging cycles. Besides both, specific power and specific energy remain constant during all the experiments (Fig. 5c). Then, the addition of IL extends the life cyclability of the material, in addition to increase all the parameters associated with the charge storage.

Some authors have proposed the manufacture of POMA supercapacitors with other materials, to increase their capacitance and their durability. Basnayaka et al. [13] manufactured supercapacitors with graphene-poly (o-anisidine) (G-POA) nanocomposites with different weight ratios of graphene to o-anisidine. The specific capacitance and C/D behavior of the POA and G-POA supercapacitors were investigated in 2 M H_2SO_4, 0.2 M $LiClO_4$, and 1 M 1-butyl-3-methylimidazolium hexafluorophosphate (BMIM-PF_6) IL. The specific capacitances

obtained were 380 F/g, 320 F/g, and 118 F/g for the 1:1 weight ratio of G-POA, POA, and G supercapacitor, respectively, in 2 M H_2SO_4 at the scan rate of 5 mV/s. However, charge/discharge measurements at a current density of 1 mA/g the G-POA-based supercapacitors showed a 27% decrease in the specific capacitance in H_2SO_4 and 16% decrease in the IL after 1000 cycles, indicating that the supercapacitors are more stable in IL electrolytes than in 2-M H_2SO_4 electrolytes. Christinelli et al. [9] evaluated by cyclic voltammetry the performance of POMA supercapacitor compared to poly(o-methoxyaniline) (POMA) and poly(3-thiophene acetic acid) (PTAA) supercapacitor fabricated by the layer-by-layer (LBL) technique in ACN with 0.1 M $LiClO_4$. The authors observed that the POMA/PTAA supercapacitor had a higher capacitance than the pristine POMA film, ranging from 50 to 140 F/g according to the number of bilayers. In another work [8], they evaluated the performance of films containing 80 μL of POMA compared to films with 60 bilayers of POMA/PTAA in ACN with 0.1 M $LiClO_4$. The charge/discharge experiments with 1.5 A/g showed that pure POMA casting film loses 80% of its capacitance after 3000 cycles; i.e., its capacitance is reduced from 98 to 22 F/g. On the other hand, the POMA/PTAA LBL film loses only 1% of its capacitance after 3000 cycles; that is, its capacitance was reduced from 99 to 98 F/g. The EIS analysis of POMA films, pure and modified, was performed to verify the influence of the different ILs on the mass transport of the dopant species, that is, the ClO_4^- counterion, and the consequent variation of the charge transfer current relative to the redox process of the conducting polymer, according to the two last reactions shown in Scheme 1. Figure 6 shows the Nyquist diagrams obtained for the four films analyzed, the respective fittings, and the equivalent circuit used for the fitting of the experimental results.

Nyquist diagrams obtained for conductive polymers typically have three distinct regions [41–43]: at high frequency, the capacitive arc represents the doping charge transfer process of the polymer film. At intermediate frequencies, the predominant mechanism is the mass transport, usually represented by the entry or exit of the counterion, according to the oxidation state

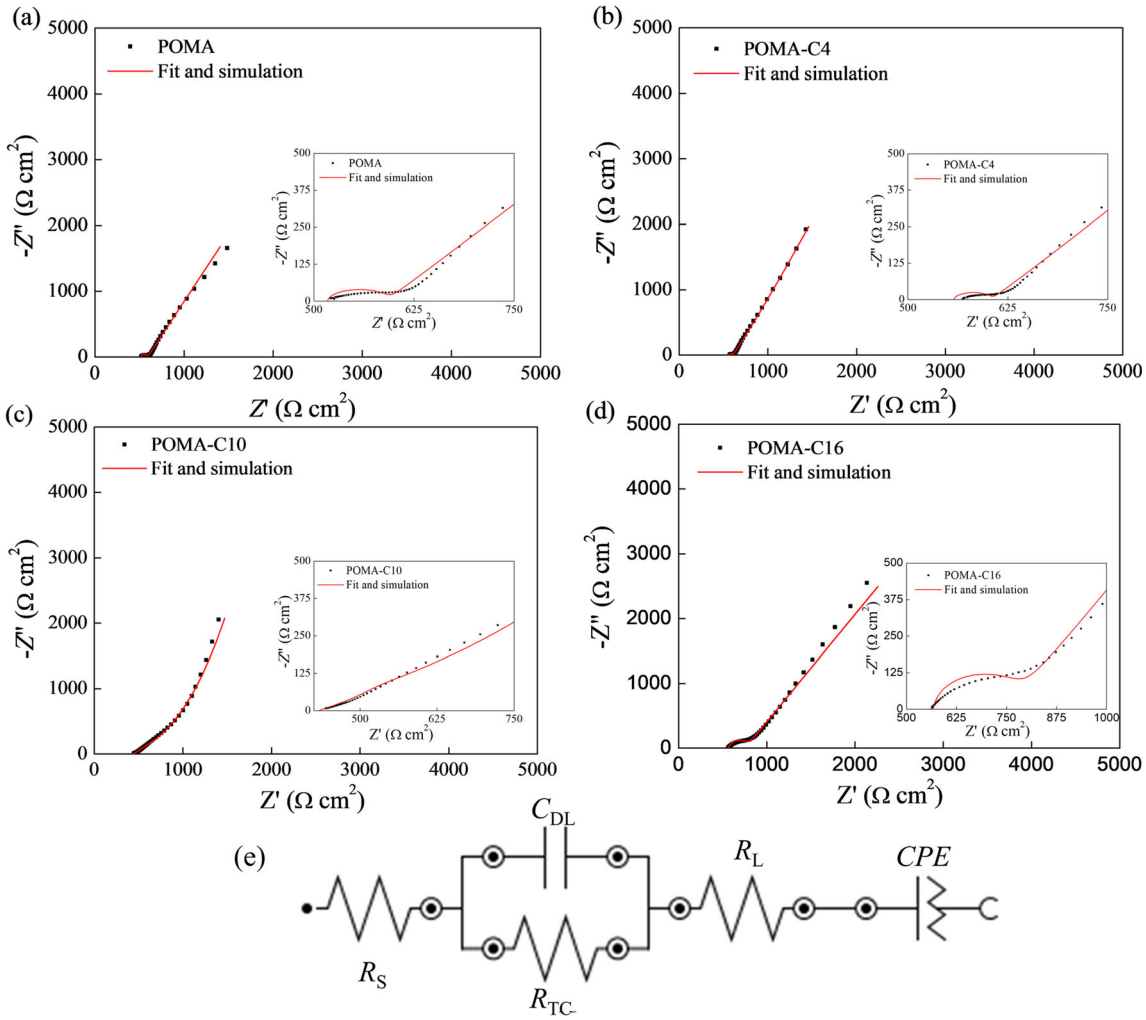

Fig. 6 Nyquist diagrams for POMA (**a**), C4-POMA (**b**), C10-POMA (**c**), and C16-POMA (**d**) films obtained in PEG with 0.1 M $LiClO_4$ in OCP and equivalent circuit used for the fitting of the experimental results (**e**)

Table 2 Impedance parameters for POMA, C4-POMA, C10-POMA, and C16-POMA films in OCP and PEG with 0.1 M $LiClO_4$

Sample	OCP (mV)	R_S (Ω/cm^2)	R_{TC} (Ω/cm^2)	C_{DL} ($\mu F/cm^2$)	R_P (Ω/cm^2)	C_P ($\mu F/cm^2$)
POMA	−69	517	144	1.33	517	160
C4-POMA	− 71	794	96	18	349	168
C10-POMA	− 48	390	216	15.1	506	76.4
C16-POMA	− 27	589	369	3.29	542	70.5

of the polymer. Finally, in the low-frequency region, the finite thickness of thin films limits the diffusion path, leading to a redox capacitance that takes place as a result of charge saturation. Therefore, the Nyquist plot shows a high-frequency capacitive arc, which describes the charge transfer process, followed by a 45° inclined line, related to the mass transport through the polymer, which changes its slope to 90°, in the region of low frequency, due to the load saturation. The OCP values are in the potential range of electrochemical activity for the POMA redox process. The experimental results for pristine POMA films, C4-POMA, C10-POMA, and C14-POMA (Fig. 6) show a capacitive arc at high frequency, followed by a straight line with a slope close to 45°, which increases inclination at low frequency. The equivalent circuit used to fit the experimental results (Fig. 6) is described as $[R_S(R_{TC}C_{DL})R_PZ_{CPE}]$. The R_S represents the unbalanced resistance at high frequency and is related to the resistance of the electrolyte between the reference electrode and the surface of the working electrode. It may also be related to the ionic conductivity of the polymer film, by the penetration of the electrolyte through pores or regions of low cross-linking in the polymer [44]. The sub-circuit ($R_{TC}C_{DL}$), related to the capacitive arc at high frequency, describes the resistance to charge transfer relative to the redox process (Fig. 4). The reaction consists of the oxidation of the leucoesmeraldine base to the emeraldine salt polaron form, with electron ejection through the metal/film interface and the ClO_4^- anion input through the film/solution interface, and consists of the charge of the capacitor. During the discharge the inverse (reduction) process occurs, with release of the anion. C_{DL} represents the double-layer capacitance at the bottom of the pore, where the electrolyte solution comes in contact with the conductive base. Due to the proximity of the relaxation times, the impedances associated to mass transport at the intermediate frequencies and to charge saturation at low frequency are overlapping. Therefore, R_P represents resistance of the polymer related to charge saturation, and Z_{CPE} (impedance of constant phase element) is related to the Warburg impedance due to injection and ejection of ClO_4^- anions during charge and discharge process, and with the capacitance due to the charge saturation of the polymer. This interpretation is justified by the value of n obtained, between 1 (pure capacitor) and 0.5 (Warburg impedance). Table 2 shows the values of the circuit elements obtained by simulation. From the admittance of the *CPE*, the polymer capacitance (C_P) was calculated by $C = Y_0^{\frac{1}{n}} R_P^{\frac{1}{n}-1}$, where Y_0 is the admittance associated with *CPE*. This capacitance therefore includes capacitance relative to mass transport and charge saturation.

The results show that the C4-POMA film presents the lowest R_{TC} value and higher C_{DL} value, evidencing that the charge transfer is facilitated in the IL medium with lower carbon chain. Likewise, this film presents the lowest value of R_P, related to mass transport, showing that the transport of the counterion during charge/discharge process is also improved. The higher C_P value also shows a more efficient charge storage for the C4-POMA film in relation to the other films tested. Therefore, the IL insertion improves the ionic conductivity of POMA, provided that its non-polar carbon chain does not influence its hydrophilic character. Films with higher ionic conductivity are more efficient in the exchange of the counterion during the redox charge/discharge process, and are indicated for the manufacture of supercapacitors. The results show that the insertion of $C_4MI.CF_3SO_3$ IL in the POMA polymer causes to capacitance to increase from 60 F/g from pristine POMA casting film to 205 F/g with the insertion of the IL (C4-POMA) with a loss of capacitance of 13% after 3000 cycles of C/D measurements at a current density of 1 A/g. The higher stability showed that the C4-POMA-based supercapacitor in PEG with 0.1 M $LiClO_4$ as compared to an aqueous electrolytic supercapacitor with POMA film opens the door for the fabrication and application of C4-POMA supercapacitors.

Conclusions

A novel material based on POMA and different IL has been prepared. The results show that the charge storage properties of the materials are dependent on the length of the alquil substituent of imidazolium ring of IL cation, and the best results were obtained for the film prepared using 1-butyl-3-methylimidazolium triflate ($C_4MI.CF_3SO_3$) together with poly(o-methoxyaniline), C4-POMA. A specific capacitance of 205 F/g was obtained for this material, which is three to five times larger than pure POMA, C10-POMA, or C16-POMA. The worst performance observed for C10-POMA and C16-POMA samples can be attributed to the fact that the $C_{10}MI.CF_3SO_3$ and $C_{16}MI.CF_3SO_3$ ILs are larger than $C_4MI.CF_3SO_3$. Their insertion into the polymer matrix may have decreased their surface area increasing the diffusional

path of counterion. The easier degradation of these films during the oxidation and reduction cycles is an indication that the reversibility in the electro-interleaving processes has been reduced. Therefore, the higher the alkyl chain attached to the imidazolium ring is, the lower the surface area of the film is, making the counterion intercalation/deinterleaving process more difficult, leading to degradation of the polymer. Charge/discharge experiments were carried out at current density of 1 A/g and showed that the material was stable for 3000 cycles. In summary, the results show that a novel material prepared by the addition of IL to the soft POMA material leads to an improvement in their charge storage properties, which is highly potential for supercapacitor applications.

Funding Financial support of this research was provided by Fundação de Amparo à Pesquisa do Estado de São Paulo (FAPESP) (Grant Nos. 2011/10897-2, 2016/05363-2, 2013/07296-2), Coordenação de Aperfeiçoamento de Pessoal de Nível Superior (CAPES), Conselho Nacional de Desenvolvimento Científico e Tecnológico (CNPq) (402287/2013-4), Sistema de Laboratórios em Nanotecnologias/Ministério da Ciência, Tecnologia e Inovação (SISNANO/MCTI), Financiadora de Estudos e Projetos (FINEP), and Embrapa AgroNano research network.

Publisher's note Springer Nature remains neutral with regard to jurisdictional claims in published maps and institutional affiliations.

References

1. Snook GA, Kao P, Best AS (2011) Conducting-polymer-based supercapacitor devices and electrodes. J Power Sources 196(1):1–12
2. Liu W, Song M-S, Kong B, Cui Y (2017) Flexible and stretchable energy storage: recent advances and future perspectives. Adv Mater 29(1):1603436
3. Shi Y, Peng L, Ding Y, Zhao Y, Yu G (2015) Nanostructured conductive polymers for advanced energy storage. Chem Soc Rev 44(19):6684–6696
4. Bryan AM, Santino LM, Lu Y, Acharya S, D'Arcy JM (2016) Conducting polymers for Pseudocapacitive energy storage. Chem Mater 28(17):5989–5998
5. Liewa C-W, Arifin KH, Kawamura J, Iwai Y, Ramesha S, Arof AK (2017) Effect of halide anions in ionic liquid added poly(vinyl alcohol)-based ion conductors for electrical double layer capacitors. J Non-Cryst Solids 458:97–106
6. Eftekhari A, Li L, Yang Y (2017) Polyaniline supercapacitors. J Power Sources 347:86–107
7. Inzelt G (2011) Rise and rise of conducting polymers. J Solid State Electrochem 15(7-8):1711–1718
8. Christinelli WA, Gonçalves R, Pereira EC (2016) Optimization of electrochemical capacitor stability of poly(o-methoxyaniline)-poly(3-thiophene acetic acid) self-assembled films. Electrochim Acta 196:741–748
9. Christinelli WA, Gonçalves R, Pereira EC (2016) A new generation of electrochemical supercapacitors based on layer-by-layer polymer films. J Power Sources 303:73–80
10. Gonçalves R, Christinelli WA, Trench AB, Cuesta A, Pereira EC (2017) Properties improvement of poly(o-methoxyaniline) based supercapacitors: experimental and theoretical behaviour study of self-doping effect. Electrochim Acta 228:57–65
11. Yang X, Wang G, Wang R, Li X (2010) A novel layered manganese oxide/poly(aniline-co-o-anisidine) nanocomposite and its application for electrochemical supercapacitor. Electrochim Acta 55(19):5414–5419
12. Mohammadi A, Peighambardoust SJ, Entezami AA, Arsalani N (2017) High performance of covalently grafted poly(o-methoxyaniline) nanocomposite in the presence of amine-functionalized graphene oxide sheets (POMA/f-GO) for supercapacitor applications. J Mater Sci Mater Electron 28:5776–5787
13. Basnayaka PA, Ram MK, Stefanakos L, Kumar A (2013) High performance graphene-poly (o-anisidine) nanocomposite for supercapacitor applications. Mater Chem Phys 141(1):263–271
14. Soares BG (2018) Ionic liquid: a smart approach for developing conducting polymer composites: a review. J Mol Liq 262:8–18
15. Watanabe M, Thomas ML, Zhang S, Ueno K, Yasuda T, Dokko K (2017) Application of ionic liquids to energy storage and conversion materials and devices. Chem Rev 117(10):7190–7239
16. Pandey GP, Hashmi SA (2013) Ionic liquid 1-ethyl-3-methylimidazolium tetracyanoborate-based gel polymer electrolyte for electrochemical capacitors. J Mater Chem A 1(10):3372–3378
17. Liu H, Yu H (2018) Ionic liquids for electrochemical energy storage devices applications. J Mater Sci Technol. https://doi.org/10.1016/j.jmst.2018.10.007
18. Marsousi S, Karimi-Sabet J, Moosavian MA, Amini Y (2019) Liquid-liquid extraction of calcium using ionic liquids in spiral microfluidics. Chem Eng J 356:492–505
19. Deyab MA (2018) Ionic liquid as an electrolyte additive for high performance lead-acid batteries. J Power Sources 390:176–180
20. Díaz M, Ortiz A, Ortiz I (2014) Progress in the use of ionic liquids as electrolyte membranes in fuel cells. J Membr Sci 469:379–396
21. Miao L, Zhu D, Liu M, Duan H, Wang Z, Lv Y, Xiong W, Zhu Q, Li L, Chai X, Gan L (2018) Cooking carbon with protic salt: nitrogen and sulfur self-doped porous carbon nanosheets for supercapacitors. Chem Eng J 347:233–242
22. Miao L, Zhu D, Liu M, Duan H, Wang Z, Lv Y, Xiong W, Zhu Q, Li L, Chai X, Gan L (2018) N, S co-doped hierarchical porous carbon rods derived from protic salt: facile synthesis for high energy density supercapacitors. Electrochim Acta 274:378–388
23. Galiński M, Lewandowski A, Stępniak I (2006) Ionic liquids as electrolytes. Electrochim Acta 51(26):5567–5580
24. Zhu Q, Song Y, Zhu X, Wang X (2007) Ionic liquid-based electrolytes for capacitor applications. J Electroanal Chem 601(1-2):229–236
25. Ketabi S, Decker B, Lian K (2016) Proton conducting ionic liquid electrolytes for liquid and solid-state electrochemical pseudocapacitores. Solid State Ionics 298:73–79
26. Kim J, Kim S (2014) Surface-modified reduced graphene oxide electrodes for capacitors by ionic liquids and their electrochemical properties. Appl Surf Sci 295:31–37
27. Mattoso LHC, MacDiarmid AG, Epstein AJ (1994) Controlled synthesis of high molecular weight polyaniline and poly(o-methoxyaniline). Synth Met 68(1):1–11
28. Dupont J, Consorti CS, Suarez PAZ, de Souza RF (2002) Preparation of 1-butyl-3-methyl imidazolium-based room temperature ionic liquids. Org Synth 79:236–243
29. Suarez PAZ, Dullius JEL, Einloft S, de Souza RF, Dupont J (1996) The use of new ionic liquids in two-phase catalytic hydrogenation reaction by rhodium complexes. Polyhedron 15(7):1217–1219
30. Pohlmann S, Olyschläger T, Goodrich P, Vicente JA, Jacquemin J, Balducci A (2015) Azepanium-based ionic liquids as green electrolytes for high voltage supercapacitors. J Power Sources 273:931–936
31. Motheo AJ, Pantoja MF, Venancio EC (2004) Effect of monomer ratio in the electrochemical synthesis of poly(aniline-co-o-methoxyaniline). Solid State Ionics 171(1-2):91–98
32. Zhu D, Jiang J, Sun D, Qian X, Wang Y, Li L, Wang Z, Chai X, Gan L, Liu M (2018) A general strategy to synthesize high-level N-

doped porous carbons via Schiff-base chemistry for supercapacitors. J Mater Chem A 6(26):12334–12343
33. Sui J, Zhang L, Peng H (2013) Label-free DNA sensor construction using self-assembled poly(o-methoxyaniline) hollow nanospheres. Eur Polym J 49(1):139–146
34. Rall JD, Seehra MS (2012) The nature of the magnetism in quasi-2D layered α-Ni(OH)2. J Phys Condens Matter 24:8
35. Mamma K, Siraj K, Meka N (2013) Effect on poly($C_6H_5NH_2$) emeraldine salt by $FeCl_3$ and $KMnO_4$ as secondary dopants. Am J Polym Sci Eng 1:1–13
36. Arof AK, Kufian MZ, Syukur MF, Aziz MF, Abdelrahman AE, Majid SR (2012) Electrical double layer capacitor using poly(methyl methacrylate)eC4BO8Li gel polymer electrolyte and carbonaceous material from shells of Mata kucing (Dimocarpus longan) fruit. Electrochim Acta 74:39–45
37. Pandey GP, Kumar Y, Hashmi SA (2011) Ionic liquid incorporated PEO based polymer electrolyte for electrical double layer capacitors: a comparative study with lithium and magnesium systems. Solid State Ionics 190(1):93–98
38. Kumbhar VS, Lokhande AC, Gaikwad NS, Lokhande CD (2015) Porous network of samarium sulfide thin films for supercapacitive application. Mater Sci Semicond Process 33:136–139
39. Christinelli WA, da Trindade LG, Trench AB, Quintans CS, Paranhos CM, Pereira EC (2017) Energy 141:1829–1835
40. Ćirić-Marjanović G (2013) Recent advances in polyaniline research: polymerization mechanisms, structural aspects properties and applications. Synth Met 177:1–47
41. Hunter TB, Tyler PS, Smyrl WH, White HS (1987) Impedance analysis of poly(vinyferrocene) films: the dependence of diffusional charge transport and exchange current density on polymer oxidation state. J Electrochem Soc 134:2198–2204
42. Ren X, Pickup PG (1997) An impedance study of electron transport and electron transfer in composite polypyrrole + polystyrenesulphonate films. J Electroanal Chem 420(1-2): 251–257
43. Bandeira MCE, Franco CV, Martini EMA (1999) Electrochemical impedance spectroscopy of poly{pyrrole-trans-[$RuCl_2(pmp)_4$]} copolymer films deposited on platinum electrodes. J Solid State Electrochem 3(4):210–214
44. Amirudin A, Thierry D (1995) Application of electrochemical impedance spectroscopy to study the degradation of polymer-coated metals. Prog Org Coat 26(1):1–28